Lithosphere

Research Article

Characteristics of Radiogenic Heat Production of Widely Distributed Granitoids in Western Sichuan, Southeast Tibetan Plateau

Chao Zhang [iD],[1,2] **Qingda Feng** [iD],[3] **Linyou Zhang,**[3] **Song Qin,**[4] **Guangzheng Jiang,**[1,2] **Jie Hu,**[1] **Shengbiao Hu,**[5] **Ronghua Huang,**[2] **and Haozhu Zhang**[2]

[1]*State Key Laboratory of Oil and Gas Reservoir Geology and Exploitation, Chengdu University of Technology, Chengdu 610059, China*
[2]*College of Energy, Chengdu University of Technology, Chengdu 610059, China*
[3]*Center for Hydrogeology and Environmental Geology Survey, China Geological Survey, Baoding 071051, China*
[4]*Regional Geological Survey Team of Sichuan Geology and Mineral Bureau, Chengdu 610213, China*
[5]*State Key Laboratory of Lithospheric Evolution, Institute of Geology and Geophysics, Chinese Academy of Sciences, Beijing 100029, China*

Correspondence should be addressed to Chao Zhang; zhangchao1113@outlook.com
and Qingda Feng; fengqingda@mail.cgs.gov.cn

Investigating the genesis of geothermal resources requires a thorough understanding of the heat source mechanism, which is also a vital basis for the efficient exploration and utilization of geothermal resources. Situated in the eastern Himalayan syntax, western Sichuan is considered to be one of the main concentration regions of high-temperature geothermal resources in China. To date, various studies have been carried out to reveal the heat source and genesis of the abundant high-temperature resources in this area; however, studies on the contribution of the radioactive heat generated by the widely distributed granitoids to the high-temperature geothermal resources remain scarce. In order to resolve this knowledge gap, we attempted to obtain evidence from the geochemical data published in the literature in the past few decades. A total of 548 radiogenic heat production rate data were determined. The statistical data indicate that the average concentrations of the heat-producing elements U, Th, and K are 6.09 ± 5.22 ppm, 26.74 ± 16.78 ppm, and $3.51 \pm 0.82\%$, respectively. The calculated heat production values of the granitoids vary from 0.52 to 10.86 $\mu W/m^3$, yielding an arithmetic average value of 3.74 ± 2.15 $\mu W/m^3$, which is higher than that of global Mesozoic–Cenozoic granites (3.09 ± 1.62 $\mu W/m^3$). Based on the heat production values, the capacity of the granitic batholiths to store heat was assessed, and the Dongcuo pluton was found to be the largest heat reservoir (382.88×10^{13} J/a). The distribution of the crustal heat flow was examined using the calculated heat production data and the stratigraphic structure obtained via deep seismic sounding in the study area. The results indicate that the crustal heat flow is 48.3–56.2 mW/m^2, which is mainly contributed by the radioactive decay in the granitoids in the upper crust. The fact that it accounts for nearly half of the regional background heat flow indicates that the radiogenic heat from the granitoids is an important heat source for the formation of the thermal anomaly and the high-temperature geothermal resources in the study area. Thus, the results obtained in this study highlight the importance of the widely distributed granitoids to high-temperature geothermal resources in western Sichuan.
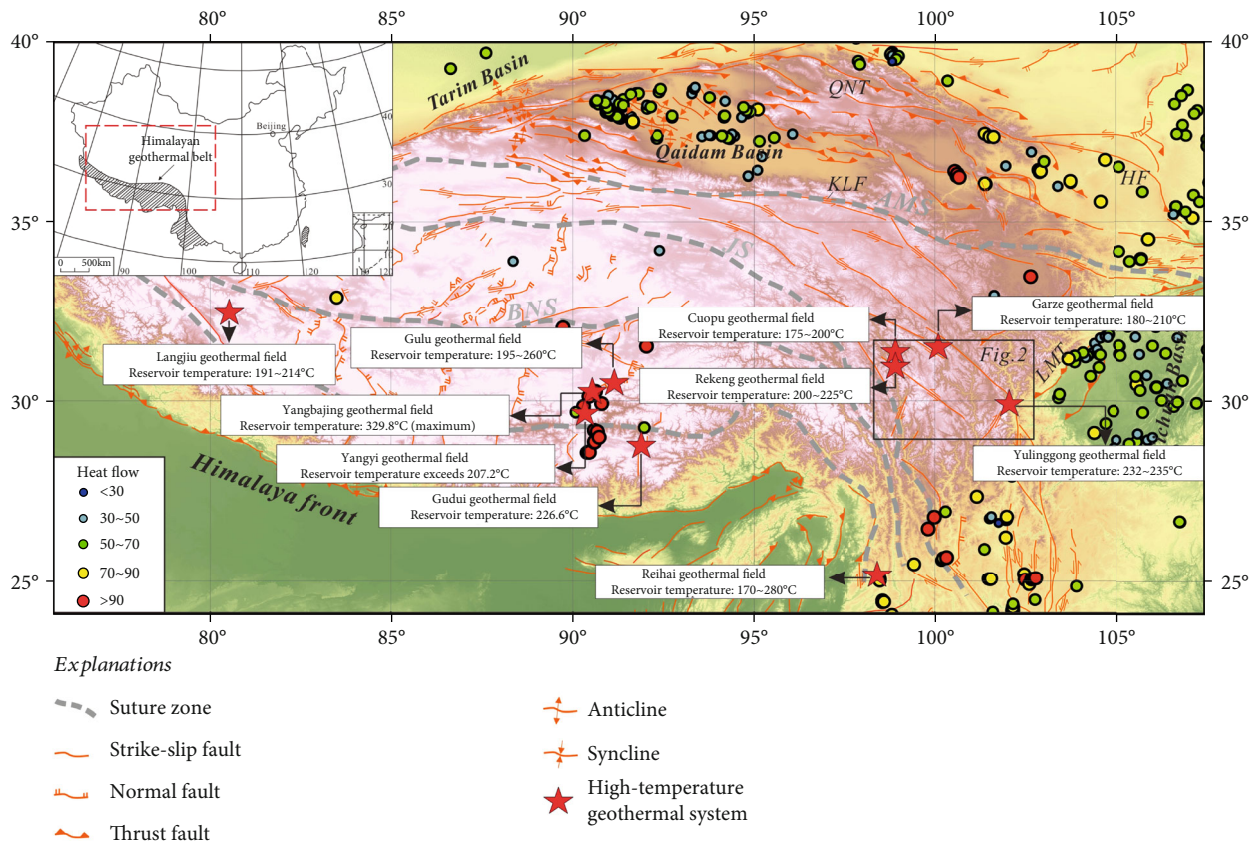
FIGURE 1: The distribution of the representative high-temperature geothermal systems in the southern Tibet–western Sichuan–western Yunnan geothermal belt (modified after Zhang et al. [12]).

1. Introduction

Geothermal resources, which are originated from the heat stored in the rocks and water within the interior of the Earth [1], are a type of green energy characterized by low-carbon emissions, a stable supply, large reserves, and a wide distribution [2]. Vigorously, developing geothermal resources can make a major contribution to carbon neutrality. A comprehensive understanding of the formation mechanism of geothermal resources is an important basis for their efficient development and utilization.

As a part of the Mediterranean–Himalayan geothermal belt, western Sichuan contains abundant high-temperature geothermal resources (Figure 1) [3], and many famous high-temperature geothermal systems are located in this area (e.g., the Rekeng and Cuopu geothermal fields in the Batang area, and the Yulingon geothermal field in the Kangding area). To determine the heat source and origin of the high-temperature geothermal resources in this area, many scientists have carried out various studies over the past few years. Based on isotope analysis of geothermal fluids, Tian et al. [4, 5] concluded that the Rekeng and Cuopu geothermal systems do not contain a mantle-derived magma chamber, and they suggested that the heat generated via crustal deformation may be the main cause of the high-temperature geothermal resources. Fan et al. [6] reached a similar nonmagmatic heat source conclusion for the Garze

geothermal system, which was further proven by Cheng et al. [7] through three-dimensional magnetotelluric inversion. Li et al. [8] deemed the lack of acid springs in the Kangding geothermal field to be attributed to a deep-seated magma chamber, which may be located in the Yulingong area in the southern part of Kangding County. An analogous finding was also reported by Cheng et al. [9], that is, there is a significantly low resistivity anomaly (less than 10 Ωm) at a depth of 10 km beneath the Kangding geothermal field. Except for the Kangding geothermal field, Zhang et al. [10] speculated that the fish shaped low-velocity zone (<3.2 km/ s, with a length of 200 km) at the depths of 15–30 km in the seismic velocity structure between Batang and Yajiang counties may represent partial melting of high-temperature materials in the crust. In addition, through numerical simulation, Ai et al. [11] investigated the effect of the shear frictional heat generated by the Xianshui River fault and concluded that shear frictional heat is the main source of the local thermal anomalies along the Xianshui River fault zone.

The general understanding of the heat sources and origins of the high-temperature geothermal resources in western Sichuan is being continuously improved through ongoing improvement of research level and investigation methods. However, virtually all of the earlier investigations disregarded the radioactive heat emanating from the granitoids, which are widely distributed in western Sichuan. Given

the significant role that granitoids have played as a source of heat throughout the development of the world's high-temperature geothermal systems, including the Qiabuqia enhanced geothermal system (EGS) field in China, the Soultz EGS field in France, and the Habanero EGS field in Australia [13–15], there is an urgent need for a scientific investigation of the thermal contribution of these granitoids to high-temperature geothermal systems.

Therefore, in this study, we obtained evidence from the data accessible in literature published in the past few decades. The main goals of this study were to determine the distribution characteristics of the radiogenic heat production rate (RHPR) of the granitoids and then to assess the radioactive heat contribution of the granitoids to the high-temperature geothermal resources. One of the key pillars of the effective development and usage of the geothermal resources in this region is the ongoing refinement of the formation mechanism of the high-temperature geothermal system in western Sichuan.

2. Geological and Geothermal Framework

Western Sichuan, located in the eastern Himalayan syntax, is in the transition zone between the Qinghai–Tibet Plateau and the Sichuan Basin (Figure 1) [3]. Structurally, western Sichuan is the junction between the Sichuan–Yunnan, Songpan–Garze, and South China active blocks, and therefore it is characterized by complex tectonic deformation and frequent seismic events [16]. Gravity inversion has shown that the crust in the study area is about 50–60 km thick [17]. Based on the magnetic inversion, the Curie isothermal surface in the study area is located at depths of 17–23 km, with an average of 20 km [18]. The Quaternary and current tectonic deformation in western Sichuan is mainly controlled by the NNW-trending and nearly NW-trending structures [19]. The Jinshajiang, Garze-Litang, and Xianshui River faults are the three major faults developed within the western Sichuan region [20]. The left-lateral strike–slip Xianshui River fault is 300 km long, and its slip rate is approximately 10–20 mm/a in the north segment and ~5 mm/a in the southern segment [19]. The Garze-Litang fault has an average velocity of 4.0 ± 1.0 mm/a. It extends from the small Maoyaba Basin, passes through the Maoyaba Basin, Litang Basin, and Kangga Basin, and finally ends to the south of Dewu [21]. Together with the Honghe fault, the Jinshajiang fault constitutes the western boundary of the Sichuan–Yunnan block, and is characterized by segmented activity; in other words, there is no obvious activity in the northern section and apparent right-lateral strike–slip movement in the middle and southern sections [22]. The aforementioned three structure systems together with the Longmenshan fault and Kangding–Yunnan fault form a "Y"-shaped tectonic area [23].

One of the most obvious features of the study area is that the geothermal activity is primarily distributed along the active fault zones (Figure 2), thus forming the Batang–Xiangcheng geothermal belt, Garze–Litang geothermal belt, and the Luhuo–Kangding geothermal belt from west to east [25]. The high-temperature reservoirs are mainly concentrated in the Rekeng (200–225°C) and Cuopu (175–200°C)

geothermal fields in Batang County, the Garze geothermal field (180–210°C), and the Yulinggong geothermal field (232–235°C) in Kangding County [4–6, 26]. The geochemical analysis conducted by Zhang et al. [27] revealed that the chemical type of the geothermal water in the study area is basically HCO_3-Na, with pH values of 6.73–9.61 and total dissolved solids values of 202.8–1649.6 mg/L. The geothermal water is recharged by snow-melt water and meteoric precipitation, with a cycle depth of 2189.93–5620.52 m [27]. Based on analysis of geothermal data, Zhang et al. [10] divided the geothermal systems in the study area into Batang and Kangding types. In both geothermal systems, meteoric water undergoes deep circulation along the fault, and then, the water rises to form hot springs after being heated by the deep heat sources [10].

The strata in the study area are predominantly Mesozoic strata, which have been intruded by large-scale granitoids (Figure 2) [27]. In the Songpan–Ganzi fold belt, the granitic plutons can be subdivided into Triassic granites with ages of 220–230 Ma, Jurassic granites with ages of 197–131 Ma, and the Cenozoic Zheduoshan granites (13–4 Ma) according to their different crystal ages [24]. The Triassic granites, which are represented by the Taiyanghe, Niuxingou, and Siguliang plutons, are believed to be related to crustal melting due to crustal thickening in the Songpan–Ganzi fold belt. Petrological studies have shown that these granitic plutons exhibit progressive development from adakite/I-type granite, high-Ba–Sr granite, A-type granite, and monzonite [28]. The Jurassic granites are mainly located near the Danba area and are characterized by S-type granites [24]. The Zheduoshan granitoids consist of earlier medium- to fine-grained granodiorite, slightly later predominated medium- to coarse-grained porphyry-like monzogranite and the latest granitoid pegmatites and aplites [29]. The geochemical data suggest that the formation of the Zheduoshan pluton was related to a low-degree of partial melting of source rocks under the Meso-Neoproterozoic continental marginal arc and the back arc basin [29]. In the Yidun volcanic arc, the crystal ages of the widely distributed granitic plutons are concentrated in four periods, 225–210 Ma, 152–102 Ma, 94–71 Ma, and 41–31 Ma [24]. The Triassic granites, which are commonly characterized by enrichment of large-ion lithophile elements and depletion of high field strength elements, are represented by the Cuojiaoma, Dongcuo, and Daocheng plutons (Figure 2) [30]. Located in the northwestern Yidun arc, the Quershan pluton (U-Pb ages of 105–102 Ma) may have been sourced from the Kangding complex in the northwestern margin of the Yangtze craton, and its formation was probably related to the closure of the Bangong–Nujiang Tethys ocean [31]. The late Cretaceous and Cenozoic granitic intrusions are mainly exposed in the western part of the Yidun arc. The representative intrusions include the Rongyicuo, Hagala, Luocuoren, and Gelie A-type granitic plutons (Figure 2). The first three plutons were all formed in an extensional tectonic setting after the collision or after the orogenic period, whereas the Cenozoic Gelie pluton, which is characterized by medium-grained monzonitic granite and a U-Pb age of 9.52 Ma, was formed in the Himalayan period [32].

FIGURE 2: Simplified geothermal-geological map of western Sichuan (modified after Tang et al. [24]) and the corresponding distributions of the RHPR data for the granitoids. JSS: Jinsha suture; GZ-LTS: Garze–Litang suture; XSHF: Xianshui River fault; LMSF: Longmenshan fault.

3. Data and Calculation Methods

The RHPR(A), which represents the heat generation capacity of the decay of the radiogenic isotopes (^{232}Th, ^{235}U, ^{238}U, and ^{40}K) in the rocks, can be determined as follows [33]:

$$A = 0.01\rho(9.52C_u + 2.56C_{Th} + 3.48C_K), \tag{1}$$

where ρ is the density of granitic rock (g/cm^3), and is assigned to be a commonly used value of 2.7 g/cm^3 in this study [34]. C_u, $C_{Th,}$ and C_K are the concentrations of uranium, thorium, and potassium (ppm, ppm, and %), respectively. To characterize the detailed distribution of the RHPRs of the granitoids, the major and trace element data for the main granitic plutons were collected, including the SiO$_2$, K$_2$O, Th, and U contents. The whole-rock major and trace element analyses were commonly conducted via X-ray fluorescence spectrometry (XRF) and inductively coupled plasma-mass spectroscopy (ICP-MS), respectively. To obtain the K content, the K$_2$O content was multiplied to a coefficient of 0.83, which was calculated from the molar masses of K and O [12]. Similar studies have been carried out in regions such

as the Gonghe Basin in China [12], the Sierras de Córdoba in Argentina [35], and the Fennoscandian Shield in Finland [36]. A total of 548 sets of data were collected for the RHPR determination, the locations of which are shown in Figure 2. Figure 2 shows that the collected data almost completely cover the main granitic plutons in the study area. Table 1 presents the contents of the radiogenic isotopes and the RHPRs of the main granitic plutons in western Sichuan calculated using Equation (1). As is shown, there are relatively large variations in the Th, U, and K contents, which range from 3 to 99.3 ppm, from 0.79 to 32.2 ppm, and from 0.15 to 6.09 wt%, respectively. In contrast, the SiO$_2$ content have a relative narrow range of 53.1–79.7 wt%.

To further determine the magnitude of the radioactive production per year of the intrusive rock bodies, it was assumed that each intrusion was characterized by a cylindrical root and its volume could be calculated by multiplying the actual outcrop area by the thickness of the root [35, 37]. Then, the radioactive heat reservoirs were estimated as follows:

$$Q = A \times \rho \times S \times H \times 10^{15} \times 10^{-6}, \tag{2}$$

TABLE 1: The contents of the radiogenic isotopes and the corresponding RHPRs of the main granitic plutons in western Sichuan.

Intrusions	U (ppm)		Th (ppm)		K (%)		SiO$_2$ (%)		A (μW/m^3)	
	Range	Mean ± SD	Range	Mean ± SD	Range	Mean ± SD	Range	Mean ± SD	Range	Mean ± SD
Zheduoshan	1.44~13.88	5.82 ± 3.13	7.4~95.8	44.93 ± 26.8	2.39~5.97	4.29 ± 0.87	70.1~76.82	72.88 ± 1.64	1.20~9.38	5 ± 2.36
Queershan	1.73~18.5	8.56 ± 3.82	16.97~99.3	46.21 ± 17.64	2.37~4.99	4.13 ± 0.44	63.29~77.69	74.47 ± 2.21	1.84~10.72	5.78 ± 1.7
Luocuoren	2.24~32.2	16.05 ± 7.43	3.17~58.4	29.08 ± 14.61	1.82~5.13	4.09 ± 0.68	69.85~79.68	75.51 ± 2	0.99~9.78	6.52 ± 1.98
Xiasai	7.46~14.05	10.95 ± 2.79	27.6~46.4	37.38 ± 7.21	3.77~4.26	4.04 ± 0.18	72.94~74.98	73.59 ± 0.75	4.22~6.78	5.78 ± 1.16
Maxionggou	6.16~12.31	8.6 ± 2.28	34.27~62	42.53 ± 9.81	3.55~5.3	3.94 ± 0.67	71.69~73.86	73.23 ± 0.8	4.3~7.95	5.52 ± 1.28
Xiuwacu	6.95~26.2	16.93 ± 7.46	23.44~50.55	37.49 ± 10.08	3.35~4.81	4 ± 0.43	70.59~78.71	75.08 ± 2.63	3.78~10.12	7.32 ± 2.41
Xilizai	2.58~8.26	6.12 ± 2.65	15.9~21.3	17.73 ± 2.43	3.38~3.73	3.59 ± 0.15	72.5~76.4	73.63 ± 1.87	2.11~3.62	3.13 ± 0.7
Daocheng	1.69~8.14	3.85 ± 1.68	9.2~44.3	21.01 ± 7.69	1.16~4.08	3.2 ± 0.72	56.34~77.14	71.1 ± 6.04	1.46~5.51	2.74 ± 0.91
Xizengqionglong	2.39~9.97	3.98 ± 1.84	3.65~7.55	5.66 ± 1.29	3.22~4.43	3.95 ± 0.35	72.42~74.88	73.83 ± 0.73	1.35~3.49	1.79 ± 0.52
Lizexi	1.74~3.54	2.38 ± 0.57	13.7~21.3	16.49 ± 2.5	2.35~3.21	2.79 ± 0.28	70.7~73.46	71.81 ± 0.99	1.74~2.66	2.01 ± 0.31
Mengtonggou	1.72~13.8	5.21 ± 3.49	13~26.5	17.5 ± 4.9	2.39~3.62	2.97 ± 0.43	70.4~75	71.42 ± 1.34	1.57~5.63	2.83 ± 1.19
Songlingkou	1.25~3.12	2.08 ± 0.6	6.9~25.8	16.32 ± 6.48	1.61~3.64	2.8 ± 0.75	56.56~68.99	62.91 ± 4.08	0.95~2.85	1.93 ± 0.64
Manai	1.98~2.75	2.38 ± 0.27	4.79~24	16.1 ± 6.79	2.64~3.32	2.95 ± 0.28	56.9~61.2	59.22 ± 1.42	1.26~2.56	2 ± 0.47
Dongcuo	1.36~12.8	4.13 ± 2.21	6.24~42.51	19.67 ± 6.2	0.15~4.55	3.27 ± 0.87	60.51~79.66	73.79 ± 3.03	1.06~5.84	2.73 ± 0.92
Yanggong	1.19~3.61	2.76 ± 0.87	5.86~26.66	15.52 ± 6.24	2.79~3.55	3.06 ± 0.32	66.9~74.15	69.68 ± 2.6	1.01~2.79	2.07 ± 0.52
Linong-Beiwu	1.92~9.32	4.19 ± 1.31	13~65.2	20.58 ± 10.15	1.57~3.62	2.89 ± 0.41	64.53~73.49	67.59 ± 2.13	1.81~6.68	2.77 ± 0.88
Sucuoma	0.79~7.97	3.56 ± 2.23	3.2~59.2	23.76 ± 17.65	0.82~4.32	2.85 ± 1.14	60.56~74.45	67.79 ± 5.3	0.5~5.94	2.83 ± 1.84
Jiaduocuo	1.07~1.67	1.29 ± 0.27	11.2~15	12.98 ± 1.57	2.14~2.61	2.39 ± 0.2	66.73~72.26	69.26 ± 2.6	1.29~1.6	1.45 ± 0.14
Dingtianzhu	3.94	3.94	17.93	17.93	3.1	3.1	61.56	61.56	2.54	2.54
Hagala	6.11~28	13.51 ± 4.84	27.95~65.8	44.54 ± 9.73	3.4~5.84	4.16 ± 0.48	69.85~77.4	73.91 ± 2.44	4.25~10.53	6.94 ± 1.57
Rongyicuo	6.16~21.9	13.58 ± 7.78	36.2~69.4	52.6 ± 12.53	4.01~4.6	4.24 ± 0.27	73.07~75.41	74.37 ± 0.94	4.5~10.86	7.52 ± 2.81
Gelie	4.07	4.07	51.9	51.9	4.25	4.25	73.81	73.81	5.03	5.03
Siguniang	5.42~15.5	9.88 ± 3.45	25~48.7	33.03 ± 8.09	3.78~4.49	4.06 ± 0.27	68.9~73.6	71.36 ± 2.07	3.54~7.76	5.2 ± 1.37
Cilincuo	6.9~22.2	12.38 ± 7.19	42.6~57.97	47.93 ± 7.2	2.51~4.3	3.48 ± 0.75	72.56~76.74	75.2 ± 1.83	5.02~9.45	6.82 ± 2.18
Taiyanghe	0.83~2.68	1.89 ± 0.38	21.8~56.9	42.69 ± 8.46	1.67~3.99	2.66 ± 0.8	53.1~73.84	58.9 ± 6.28	2.1~4.62	3.69 ± 0.58
Cuomolong	2.54~8.14	5.63 ± 2.84	12.03~26.12	21.3 ± 8.03	3.51~6.09	4.55 ± 1.36	71.58~75.09	73.83 ± 1.95	1.86~4.47	3.35 ± 1.34
Jiajika	2.1~8.79	4.05 ± 2.03	3~4.08	3.56 ± 0.45	3.76~4.24	4 ± 0.15	73.93~75.06	74.57 ± 0.39	1.11~2.82	1.66 ± 0.51
Yongjie	1.79~4.03	2.71 ± 0.93	12.1~19.5	15.67 ± 3.06	2.35~3.14	2.86 ± 0.29	69.68~71.72	70.58 ± 0.8	1.62~2.67	2.05 ± 0.38
Laojungou	2.29~8.23	3.99 ± 1.52	14.5~34.2	20.51 ± 5.56	2.57~3.99	3.36 ± 0.44	63.9~72.7	69.29 ± 2.3	2.06~3.79	2.76 ± 0.59
Maerkang	2.94~8.53	14.54 ± 5.65	5.34~25.22	4.39 ± 1.72	2.97~4.59	3.99 ± 0.43	69.57~74.74	73.3 ± 1.45	1.73~3.57	2.51 ± 0.57
Niuxingou	2.85~8.1	4.3 ± 2.01	6.44~39	19.84 ± 12.2	2.86~4.2	3.62 ± 0.54	53.7~63.6	59.12 ± 4.38	1.48~5.16	2.82 ± 1.35

Table 1: Continued.

Intrusions	U (ppm)		Th (ppm)		K (%)		SiO$_2$ (%)		A (μW/m^3)	
	Range	Mean ± SD	Range	Mean ± SD	Range	Mean ± SD	Range	Mean ± SD	Range	Mean ± SD
Menggu	2.08~2.75	2.39 ± 0.34	15.2~22.2	19.3 ± 3.65	3.2~3.55	3.43 ± 0.2	67.2~68	67.63 ± 0.4	1.89~2.47	2.27 ± 0.33
Tagong	1.52~3.35	2.32 ± 0.57	7.24~24.84	19.36 ± 4.99	1.97~3.4	3.03 ± 0.36	59.65~71.59	63.81 ± 2.53	1.18~2.81	2.22 ± 0.44
Maoergai	1.82~3.24	2.77 ± 0.65	10.57~14.44	12.58 ± 1.67	2.81~3.72	3.2 ± 0.38	70.63~74.09	72.15 ± 1.51	1.49~2.05	1.88 ± 0.27
Cuojiaoma	2.26~4.03	2.86 ± 0.69	16.43~25.78	19.69 ± 3.39	2.66~3.17	2.92 ± 0.2	71.24~73.44	72.65 ± 0.79	2.04~3.11	2.37 ± 0.39
Ajinsenduo	2.04~4.11	3.1 ± 0.95	16.2~19.4	18.33 ± 1.45	3.27~3.66	3.42 ± 0.18	70.73~74.78	72.12 ± 1.81	2.09~2.68	2.38 ± 0.28
Luomo	2.02~2.07	2.05 ± 0.04	10.24~20.88	15.56 ± 7.52	1.88~4.1	2.99 ± 1.57	65~72.07	68.54 ± 5	1.42~2.35	1.88 ± 0.66
Riluku	1.7~12	4.1 ± 1.9	7.56~45.2	22.1 ± 9.48	1.7~4.47	3.06 ± 0.69	59.31~75.49	69.51 ± 3.34	1.13~5.28	2.87 ± 0.95

where Q is the heat produced per year (J/a), A is the RHPR of the granitic rocks (μJ/g·a), S is the granitic outcrop surface area (km^2), and H is the vertical thickness of the intrusion (km). Due to the absence of studies on the entire geometry or the vertical extension of the granitic intrusions, a uniform thickness of 13 km was specified for each intrusion, which is similar to the thickness of the radioactively enriched layer suggested by Wang [38]. The RHPR of each intrusion was considered to be uniform; therefore, the vertical variation in the RHPR, which may be caused by fractionation, was not considered in this study, as the works of Zhou et al. [37].

4. Results and Discussion

4.1. RHPR Variations. The determined RHPRs of the granitic rocks in the western Sichuan area are shown in Figure 3. The studied granitoids are characterized by a rather wide range of RHPR values, ranging from 0.52 to 10.86 μW/m^3. The statistical data indicate that the RHPRs of 363 granitic rocks, accounting for 66.2% of all the samples, lie between 1 and 4 μW/m^3. The arithmetic mean value for all of the rocks was calculated to be 3.74 ± 2.15 μW/m^3, which is 1.87 times the average crustal value (2.04 ± 1.83 μW/m^3, [39]). Based on the complied RHPR data for granitic rocks worldwide, Artemieva et al. [34] concluded that, although there is no systematic correlation between the type of granite and the RHPR, A-type (anorogenic) granites are the most radioactive (i.e., 3.57 ± 1.72 μW/m^3 for Precambrian granites and 2.23 ± 0.81 μW/m^3 for Phanerozoic granites). Due to the commonly absent of the information on granite types in compiled literature, it is very difficult to examine the RHPR patterns associated with different types of granites in the study area. In general, the RHPR values of the granitic rocks in western Sichuan obtained in this study are higher than the average RHPR value of global Mesozoic–Cenozoic granites (3.09 ± 1.62 μW/m^3, [34]) and that of the most radioactive A-type granites. The relatively high RHPRs indicate the enrichment of radioactive elements. In addition, the RHPRs of the granites in western Sichuan are also substantially higher than those in the Gonghe Basin (3.20 ± 1.07 μW/m^3, [12]) in the northeastern Qinghai–Tibet Plateau and in Tibet (3.2 ± 1.5 μW/m^3 and 2.6 ± 1.6 μW/m^3 in southern and northern Tibet, respectively [40]). Additionally, the RHPR comparison presented in Table 2 suggests that the RHPR values in the study area are comparable with or even higher than those in several typical high-temperature geothermal areas, e.g., the Habanero high-temperature geothermal area in Australia.

The relationships between the RHPR and the concentrations of SiO$_2$ and radioelements are shown in Figures 4(a)–4(d). In general, U, Th, and K are large-ion lithophile elements and have an affinity toward the higher SiO$_2$ content [35]. This may be the reason for the roughly normal relationship between the RHPR values and SiO$_2$ contents (Figure 4(a)). This means that the granitic plutons with higher SiO$_2$ contents always possess higher concentrations of radiogenic elements and therefore have higher RHPR values. According to the data, the RHPR values increase from 1.48 μW/m^3 to 10.12 μW/m^3 as the SiO$_2$ content
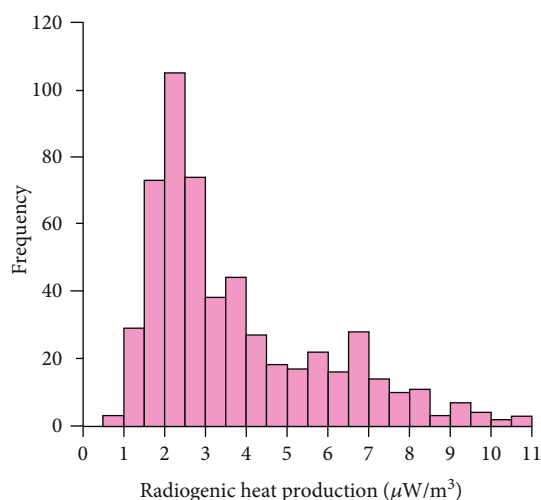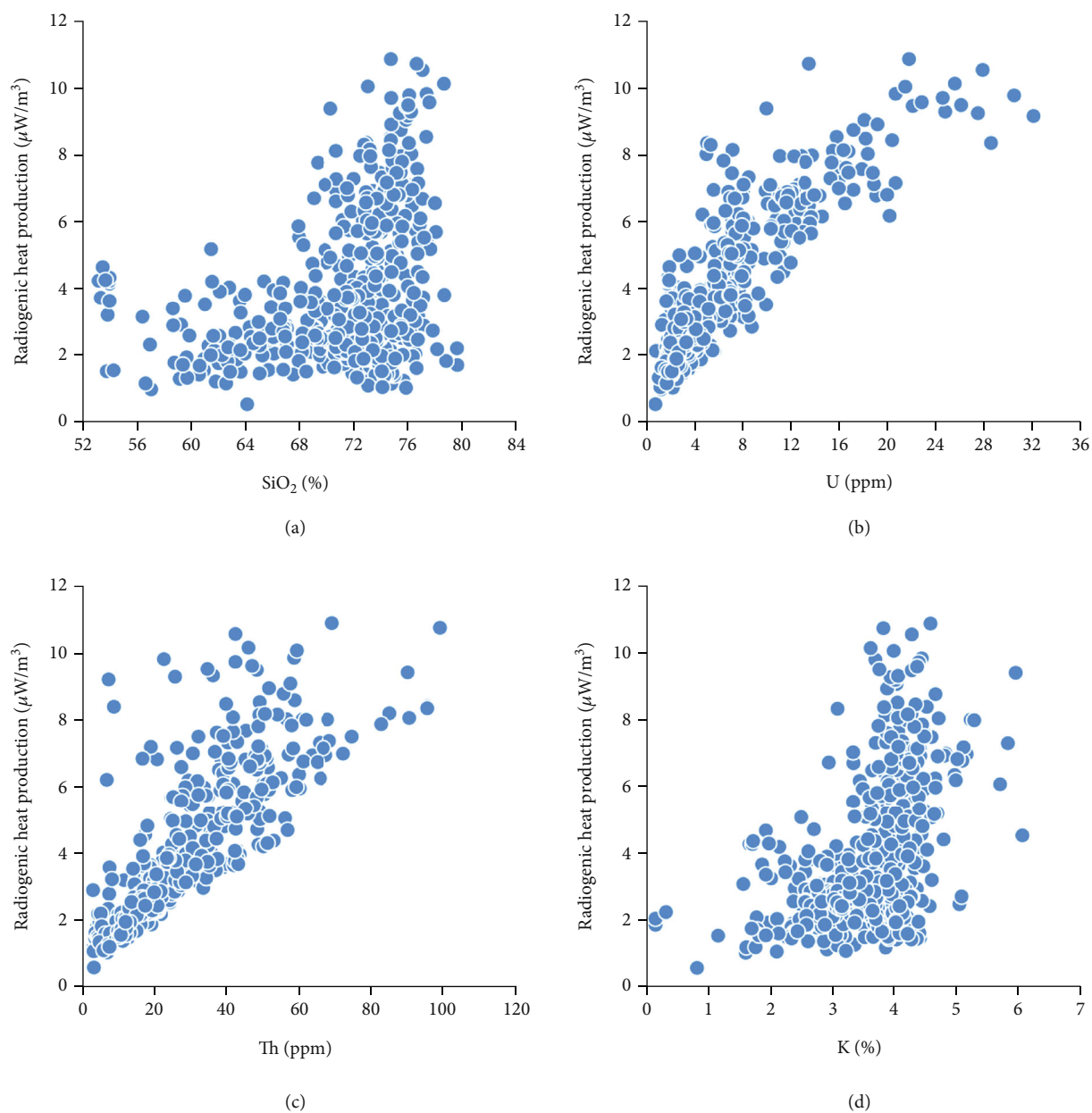

FIGURE 3: Frequency histogram of the RHPR data for the granitic rocks in western Sichuan.

increases from 53.7% to 78.68%. However, not all of the rock samples conform to this behavior. As is shown in Figure 4(a), for SiO$_2$ contents of 72–80%, the RHPRs are characterized by a wide fluctuation from about 1 μW/m^3 to 11 μW/m^3. In addition, the rock sample with maximum SiO$_2$ content (79.68%) has a low RHPR of only 1.15 μW/m^3. This phenomenon was also observed in the studies of Pleitavino et al. [35], Veikkolainen and Kukkonen [36], and Slagstad [44]. According to Kukkonen and Lahtinen [45], the reason for this phenomenon is that the U- and Th-bearing accessory minerals may start to replenish the remaining melts in the evolved magmas (>70% SiO$_2$), and the amount of heat producing elements incorporated into the melt fraction varies due to the different source compositions, melting temperatures, melt segregation rates, and environments. Consequently, a high RHPR scatter can be observed in the high-SiO$_2$ melts. In Figures 4(b)–4(d), the RHPR roughly increases for higher Th, U, and K contents. However, compared with Th and U (Figures 4(b)–4(c)), the relationship between the RHPR and the K content exhibits significant scatter (Figure 4(d)), which is consistent with the previous data reported by Pleitavino et al. [35] and Zhang et al. [12]. In terms of the relative proportions of the total heat production, the average heat contributions of U and Th are 39.3% and 49.7%, respectively, whereas the heat contribution of K only accounts for 11% (Figure 5).

The Th/U ratio is a useful parameter for the characterization of granitic rocks [34], and it can be used to reflect source variations due to the fact that this ratio does not change significantly during partial melting [46]. Taylor and McLennan [47] reported that the upper crust, middle crust, and lower crust are characterized by Th/U ratios of 3.8, 4.9, and 6.0, respectively. According to the conclusion of Artemieva et al. [34], the Th/U ratio exhibits a subtle decrease from early Proterozoic to Paleozoic granites, and the minimum value (~2.78) occurs in the Archean granites. The global average Th/U ratio value is estimated to be 4.75 ± 4.27 [34]. The study area is characterized by very high Th/U ratios of 0.23–30.76, with a mean value of 6.02 ±

TABLE 2: RHPR comparison of the granitoids in typical high-temperature geothermal fields worldwide.

Location	Areas	Time	RHPR(μW/m³)		Reference
			Ranges	Means ± SD	
China	Western Sichuan	Cenozoic-Triassic	0.52~10.86	3.74 ± 2.15	This study
China	Qiabuqia	Triassic	1.17~5.81	3.20 ± 1.07	[12]
Australia	Habanero	Carboniferous	7~10	—	[13]
France	Soultz	Hercynian	>7 (maximum)	—	[14]
Bavaria	Franconian Basin	Hercynian		4-6	[41]
Portugal	Beiras	Hercynian	—	5.5	[42]
England	Cornwall	Permian	4.5~5	—	[43]

FIGURE 4: Plots of RHPR versus the (a) SiO$_2$, (b) U, (c) Th, and (d) K contents for the granitic rocks.
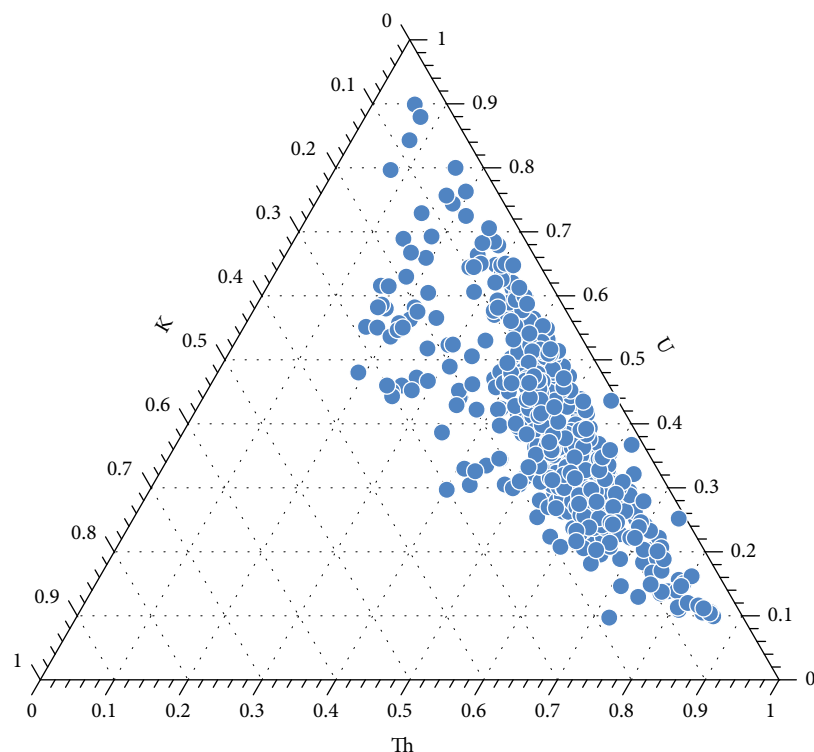
FIGURE 5: Ternary diagram of the relative radiogenic heat produced by the heat-producing elements U, Th, and K.

(a)

(b)
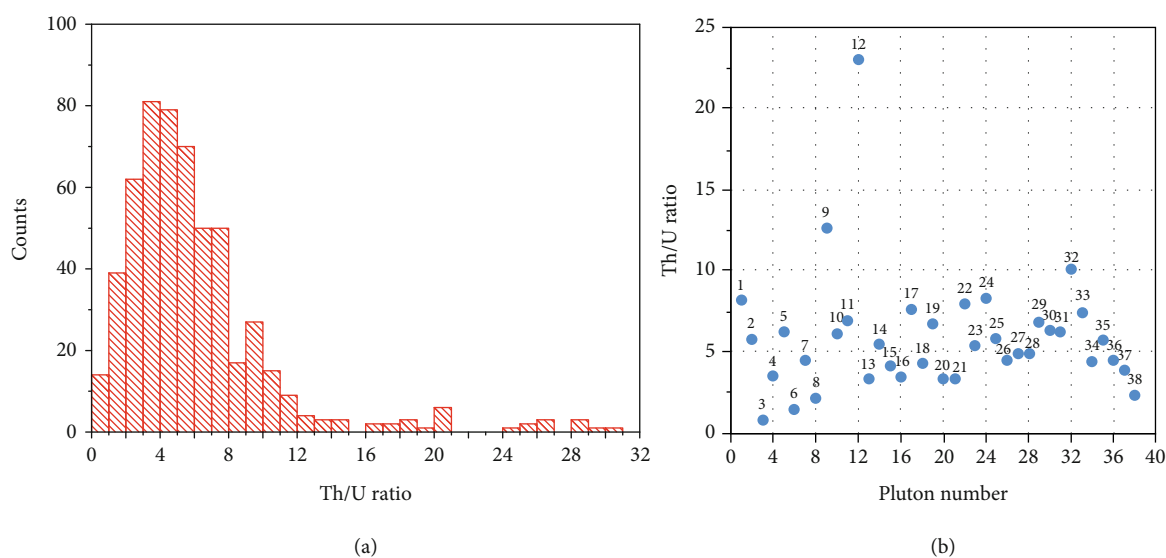
FIGURE 6: (a) Frequency histogram of the Th/U ratio of the granitic rocks and (b) the average Th/U ratio of each granitic pluton in western Sichuan. 1-Zheduoshan; 2-Daocheng; 3-Jiajika; 4-Hagala; 5-Queershan; 6-Xizengqionglong; 7-Rongyicuo; 8-Luocuoren; 9-Gelie; 10-Yongjie; 11-Lizexi; 12-Taiyanghe; 13-Xiasai; 14-Laojungou; 15-Mengtonggou; 16-Maerkang; 17-Songlingkou; 18-Niuxingou; 19-Manai; 20-Siguniang; 21-Xilizai; 22-Menggu; 23-Dongcuo; 24-Tagong; 25-Yanggong; 26-Maoergai; 27-Linong–Beiwu; 28-Maxionggou; 29-Cuojiaoma; 30-Sucuoma; 31-Ajisenduo; 32-Jiaduocuo; 33-Luomo; 34-Dingtianzhu; 35-Rihaizi; 36-Cilincuo; 37-Cuomolong; and 38-Xiuwacu.

4.63 (Figure 6(a)). If the Th/U ratio is assumed to follow a normal distribution as suggested by Artemieva et al. [34], the calculated average Th/U ratio is 4.92 ± 2.4 when the tail beyond ca. 1σ (ca. 4.6) of the normal distribution is

excluded, which may be attributed to a different mechanism of granitic magma generation compared to the normal distribution [34]. The anomalously high Th/U ratios of the Gelie and Taiyanghe plutons (Figure 6(b)) are due
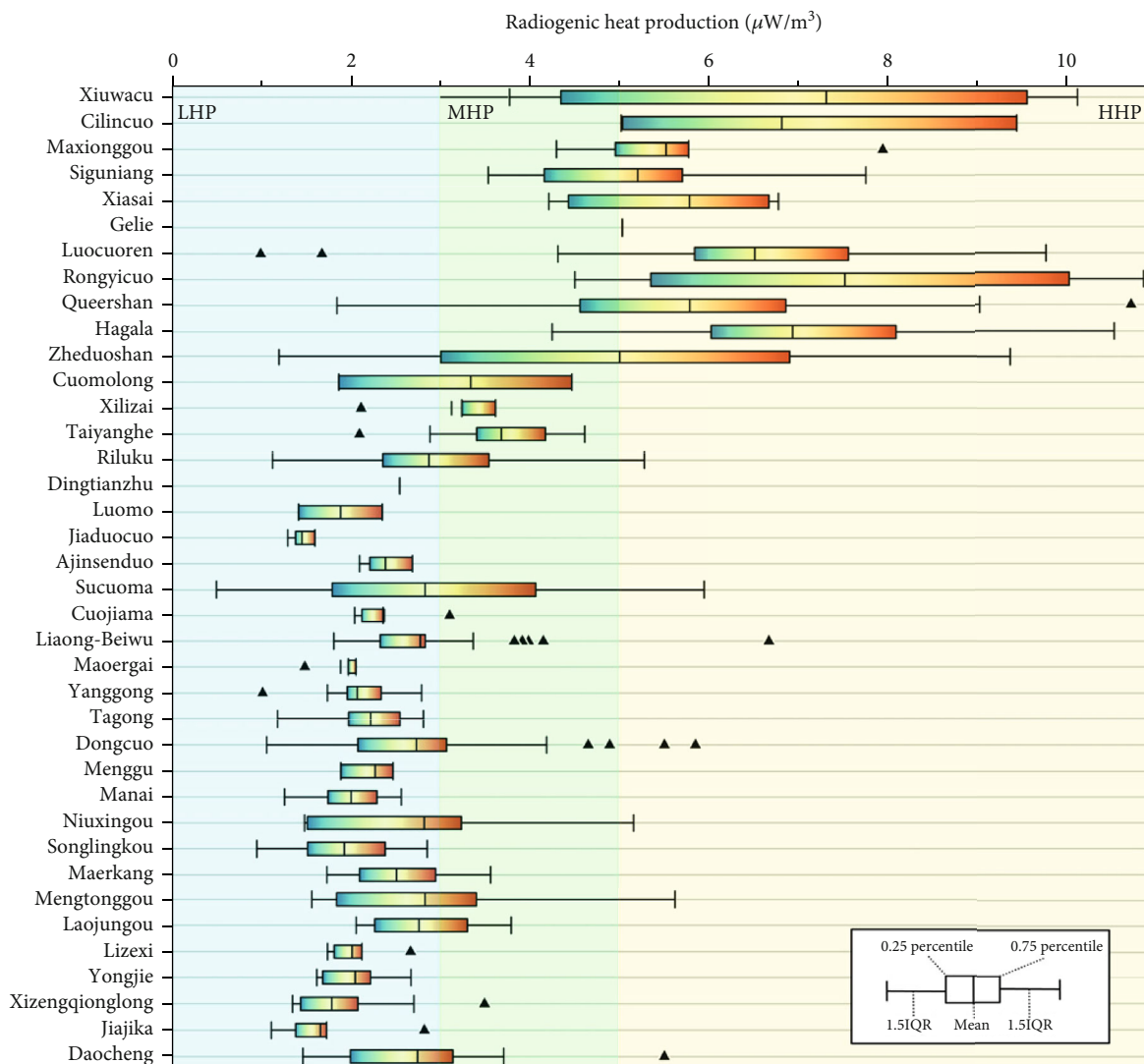
FIGURE 7: Boxplots of the RHPRs of the different granitic intrusions in western Sichuan, showing the mean values and interquartile (25–75%) ranges.

to lower U concentrations (Table 1). The possible reasons for this are different source compositions and later metasomatic processes [48].

Figure 7 and Table 1 display the RHPR variations of the main granitic intrusions in the western Sichuan region. As can be seen, the RHPRs of the various invasions differ greatly, which may be connected to the occurrences of the different magmatic events. It can be clearly seen from Figure 8 that the average RHPR values of the granitic rocks formed in the Cenozoic and Cretaceous exceed $5\,\mu W/m^3$, whereas the Jurassic and Triassic granites are characterized by relatively low average RHPR values of $2.41 \pm 0.7\,\mu W/m^3$ and $2.73 \pm 1.17\,\mu W/m^3$, respectively. As was proposed by Pleitavino et al. [35], the differences in the RHPRs of granitic rocks formed under different magmatic events may be due to the different origins and tectonic settings, which would affect their chemical compositions and the concentrations of the radioactive elements, as well as their radioactive heat generating capacities. Additionally, the chemical alterations

caused by processes such as metamorphism, metasomatism, and weathering after magma generation can also affect the concentrations of the radioactive elements [12]. Mccay and Younger [49] subdivided granites into three categories according to their RHPRs: high heat production (HHP) granites with RHPRs of greater than $5\,\mu W/m^3$, marginal heat production (MHP) granites with RHPRs of $3–5\,\mu W/m^3$, and low heat production (LHP) granites with RHPRs of less than $3\,\mu W/m^3$. Following this classification scheme, the Cenozoic Zheduoshan and Gelie intrusions, the Cretaceous Hagala, Rongyicuo, Luocuoren, and Xiasai plutons, the Jurassic Queershan pluton, and the Triassic Siguniang, Maxionggou, Cilincuo, and Xiuwacu plutons are HHP granites (Figure 7). The MMP granites include the Taiyanghe, Xilizai, and Cuomolong plutons. The remaining plutons are LHP granites. Among these plutons, the Rongyicuo pluton has the highest average RHPR value of $7.52 \pm 2.81\,\mu W/m^3$ ($N = 5$), whereas the Jiaduocuo pluton possess the lowest average RHPR value of $1.45 \pm 0.14\,\mu W/m^3$ ($N = 4$).
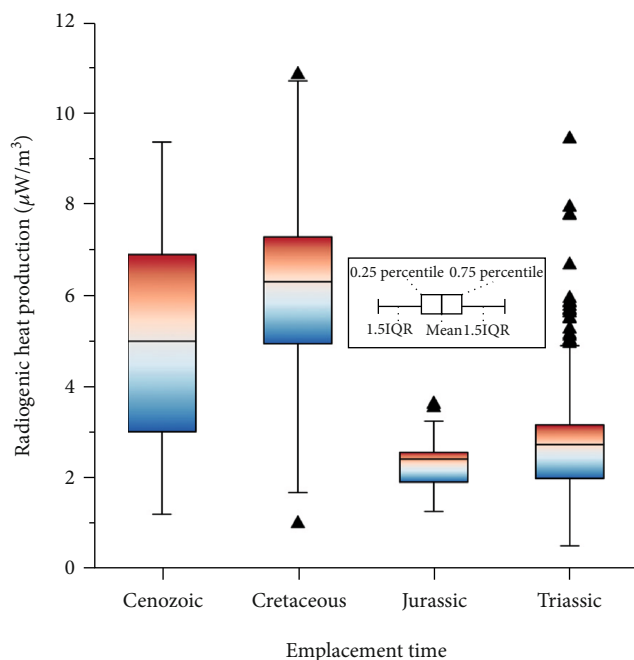
FIGURE 8: Boxplots of the RHPRs of the granitic rocks in western Sichuan according to their magmatic events.

4.2. Heat Contribution to the High-Temperature Geothermal Resources.

During the formation of high-temperature geothermal resources (or systems), the heat source is particularly important [50]. Based on research on the genesis of the high-temperature geothermal systems conducted by Zhang et al. [51], a magma chamber, radiogenic heat generated by the decay of the radioactive elements, and anomalously high-mantle heat flow are the most common heat sources. Although the granitic rocks are extensively distributed in western Sichuan (Figure 2), their impacts on the formation of the geothermal resources have not yet received sufficient attention. Thus, the main goal of this section is to analyze the role of the heat production of the widely distributed granitoids in this area in detail based on the RHPRs as discussed. To achieve this, the heat reservoirs of the granitic plutons and the vertical crustal heat flow distribution are investigated.

4.2.1. Heat Reservoirs of the Granitoids.

Using Equation (2), the magnitudes of the radioactive heat production per year of the main intrusions were calculated. Table 3 presents the main characteristic parameters of each pluton. The results show that the majority of the heat reservoirs of the granitic plutons are less than 100×10^{13} J/a. Among the 38 main plutons, 25 have heat reservoirs of less than 50×10^{13} J/a, and five possess heat reservoirs of $50–100 \times 10^{13}$ J/a. The Dongcuo pluton has the largest heat reservoir of 382.88×10^{13} J/a, and it is characterized by a mean RHPR of $2.73 \mu W/m^3$ and an outcrop area of $\sim 3329 km^2$ (Table 3). From the relationship between the heat reservoirs and RHPRs, as well as the outcrop areas (Figure 9), the heat reservoir generally increases as the mean RHPR and the outcrop surface increase. However, not all of the plutons follow

this trend. For example, the mean RHPR of the Rongyicuo pluton is the largest, but its heat reservoir is not the highest. Similar situations also encountered in other batholiths, e.g., the Cuojiaoma pluton, which has a moderate mean RHPR but the second largest heat reservoir. These interesting relationships have also been noted by Rollin [52], Mccay and Younger [49] and Pleitavino et al. [35].

4.2.2. Crustal Heat Flow Distribution.

Terrestrial heat flow is one of the most important signals for geothermal resources [38, 53]. High-temperature geothermal resource occurrence areas are always characterized by anomalous heat flow values. The most obvious evidence of this relationship is that the four global high-temperature geothermal resource belts are all characterized by high heat flow anomalies [54, 55]. The terrestrial heat flow (mW/m^2), which is commonly obtained via continuous steady-state borehole temperature logs and thermophysical parameter tests, consists of two components, namely, the radiogenic heat production from the crustal layer (Q_c) and the heat loss from the Earth's mantle (Q_m) [39]. Therefore, establishing a crustal heat flow distribution model and assessing the crustal heat flow components is the basis of determining the heat composition and thus understanding the heat source of a geothermal system.

To study the vertical heat flow distribution within the crust, a one-dimensional crustal stratigraphic column model was constructed based on the crustal seismic velocity structure of the Zhubalong–Zhizhong profile obtained via the deep seismic sounding conducted by Wang et al. [56]. Figure 10 shows the constructed crustal framework, which is 61 km thick and consists of four sections: (a) a 13 km-thick upper crustal layer, (b) a 9 km-thick low-velocity zone (LVZ), (c) an 8 km-thick middle crustal layer, and (d) a 31 km-thick lower crust. In the process of generating the crustal heat flow distribution, the RHPR distribution of each subcrustal layer is necessary. To characterize the vertical distribution of the RHPR, three models have been commonly utilized in previous studies, i.e., (a) constant heat production A_0 over depth b (representing the thickness of the radioactively enriched layer), (b) linearly decreasing heat production over depth $2b$, and (c) exponentially decreasing heat production from a surface value of A_0 with an $1/e$ fold length scale of b [57]. In this study, the RHPRs of the middle and lower crust were both assumed to follow the constant model, whereas the exponential model was specified for the upper crust [39]. For the surface value of A_0 in the upper crust, the average RHPR value determined in Section 4.1 was employed. For the middle and lower crust, the RHPRs were estimated in the first approximation using the empirical relationship between the RHPR and the compressional seismic velocity proposed by Rybach and Buntebarth [58], i.e., $\ln^A = 13.7 - 2.17 \times V_p$. Before converting the V_p into the RHPR value, the in situ V_p needs to be corrected to laboratory conditions of 20°C and 200 MPa [59].

In the Zhubalong–Zhizhong seismic profile, an LVZ with an average thickness of 9 km is present in the crustal domain in the study area [59]. Additionally, a low-

TABLE 3: The estimated heat reservoirs of the main granitic plutons in western Sichuan.

| Intrusions	Mean A (μW/m^3)	Mean Q_a (μJ/g/y)	Heat reservoir (10^{13} J/y)	Intrusions	Mean A (μW/m^3)	Mean Q_a (μJ/g/y)	Heat reservoir (10^{13} J/y)
Zheduoshan	5.00	60.16	178.37	Hagala	6.94	83.52	105.76
Queershan	5.78	69.53	174.25	Rongyicuo	7.52	90.53	47.49
Luocuoren	6.52	78.44	113.31	Gelie	5.03	60.5	138.38
Xiasai	5.78	69.51	12.46	Siguniang	5.20	62.58	70.98
Maxionggou	5.52	66.37	22.69	Cilincuo	6.82	82.09	84.18
Xiuwacu	7.32	88.06	88.16	Taiyanghe	3.69	44.34	11.64
Xilizai	3.13	37.64	22.59	Cuomolong	3.35	40.17	17.74
Daocheng	2.74	32.94	75.42	Jiajika	1.66	19.88	0.93
Xizengqionglong	1.79	21.39	4.55	Yongjie	2.05	24.59	23.70
Lizexi	2.01	24.16	2.89	Laojungou	2.76	33.14	43.01
Mengtonggou	2.83	33.97	22.09	Maerkang	2.51	30.09	34.50
Songlingkou	1.93	23.10	1.49	Niuxingou	2.82	33.81	16.96
Manai	2.00	24.01	11.06	Menggu	2.27	27.23	21.76
Dongcuo	2.73	32.77	382.88	Tagong	2.22	26.64	10.32
Yanggong	2.07	24.82	63.52	Maoergai	1.88	22.57	14.13
Linong-Beiwu	2.77	33.29	5.87	Cuojiaoma	2.37	28.46	229.31
Sucuoma	2.83	33.95	2.73	Ajinsenduo	2.38	28.61	6.78
Jiaduocuo	1.45	17.42	26.88	Luomo	1.88	22.58	3.87
Dingtianzhu	2.54	30.54	19.68	Riluku	2.87	34.46	89.87
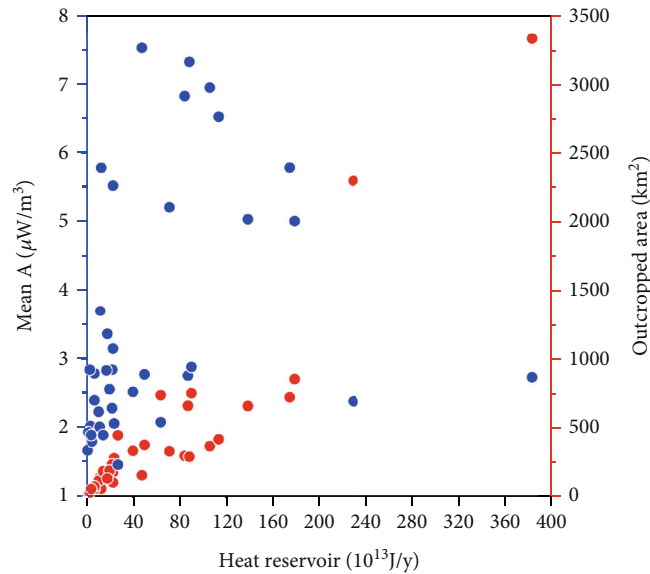
FIGURE 9: Plots of the heat reservoirs vs. the mean RHPR and outcrop area for the granitic plutons in western Sichuan.

resistivity zone (LRZ) with a magnitude of several to tens of ohm m was consistently detected by Sun et al. [60] at a similar depth as the LVZ. Wang et al. [56] attributed the coincidence of the LVZ and LRZ beneath the study area to overpressurized hydrous fluids or partial melting. In fact, such interpretation is universally accepted in analyses of geophysical profiles in the Qinghai–Tibet Plateau, such as in wide-angle reflection/refraction seismic exploration,

receiver function, seismic tomography, and magnetotelluric profiles [61]. Following the aforementioned viewpoint, the LVZ in the crust may act as an additional magma heat source expect for the crustal radioactive heat source and mantle heat source. A similar situation has been also encountered in many other high-temperature geothermal systems. For instance, Zhang et al. [12] concluded that the magmatic heat contributed by the partial melting zone at
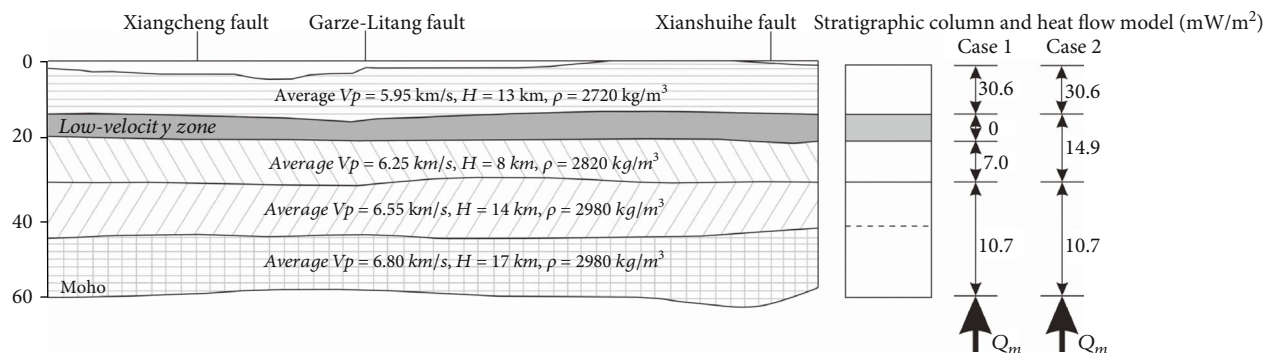
Figure 10: Crustal stratigraphic column model of western Sichuan (after Wang et al. [56]) and the radiogenic heat flow generated by each subcrustal layer.

depths of 15–35 km beneath the Qiabuqia hot dry rock (HDR) field in the Gonghe Basin is an important additional heat source.

In light of the aforementioned circumstance, two cases are considered in the following calculation process. In the first case, assuming that the magma chamber exists at the depth range of LVZ, the entire crustal heat flow can be determined by adding the radiogenic heat contributions of the upper, middle, and lower crustal layers. This case represents the minimum crustal heat flow. In the second case, the LVZ is assumed to be the normal middle crustal stratum, and thus, the radiogenic heat component generated by the LVZ can be roughly estimated by using the RHPR value of the middle crust. Therefore, the entire crustal heat flow is determined by adding the amounts of radiogenic heat of all of the crustal sections, which may represent the maximum crustal heat flow. The calculated heat flows of the subcrustal layers are demonstrated in Figure 10. As is shown, the radiogenic heat is dominated by the upper crustal section, which is about 30.6 mW/m². The middle crust contributes a gross heat flow of 7 mW/m² and 14.9 mW/m² in cases 1 and 2, respectively. The larger thickness of the lower crust leads to a larger amount of radiogenic heat of 10.7 mW/m². In total, the entire crustal section in western Sichuan generates a heat flow of 48.3–56.2 mW/m² due to radioactive decay in the crustal rocks.

4.2.3. Implications for the Heat Source and Origin of the High-Temperature Geothermal Resources. The heat reservoirs of the main granitic plutons, as well as the crustal heat flow partitioning, have been investigated in detail. This section aims at revealing the role of the granitoids in the formation of the high-temperature geothermal resources in the study area. The first task was to determine the regional background heat flow in western Sichuan. However, there are no available measured terrestrial heat flow data for western Sichuan (Figure 1) according to the latest heat flow data compilation for the Chinese mainland completed in 2016 by Jiang et al. [62]. The main reason for this may be the extreme high-altitude conditions of the study area. Thence, it was difficult to accurately obtain the background heat flow value. Given its special location (i.e., the eastern Himalayan syntax) and the strong tectonic activity, western Sichuan

has been regarded as an area characterized with a high thermal state [62, 63].

Due to the large limitations and relatively huge cost of measuring the heat flow using the traditional method, several indirect methods have been employed to estimate the heat flow values in recent years. The Curie point depth, which reflects the bottom of the magnetic sources, has been proven to be a useful parameter for estimating the temperature at depth, especially in regions where no borehole temperature logs are available. The feasibility of estimating the surface heat flow and deep thermal structure using Curie point depth data has already been discussed in many studies [64–67]. Based on Curie depth data and the concentrations of the radioactive elements, Tang et al. [68] estimated the heat flow in the southeastern Tibetan Plateau, which is shown in Figure 11. It is obvious that the entire southeastern Tibetan Plateau is characterized by a high heat flow in the southwestern region, and low heat flow in the northeastern region. According to Tang et al. [68], the estimated heat flow varies from 44 mW/m² to 108 mW/m², with an average value of 75 mW/m². Western Sichuan, which is the transition zone between the high and low heat flow areas, has relatively high heat flow values. The Batang, Litang, Kangding, Garze, Xiangcheng, and Daocheng geothermal areas in western Sichuan are all characterized by heat flows of greater than 70 mW/m², and the heat flow is even close to 100 mW/m² in some typical areas according to the heat flow distribution map (Figure 11). Thus, the regional background heat flow in western Sichuan can be reasonably set as 75–85 mW/m², which is approximately consistent with Figure 11.

Based on the crustal heat flow and the regional background heat flow in western Sichuan, the thermal contribution of the granitoids to the formation of the high-temperature geothermal resources was roughly determined. According to the results, the radiogenic heat generated by the crustal rocks contributes nearly half of the surface heat flow. According to the crustal heat flow partitioning, the heat contribution of the upper crust is very large, accounting for 54.4–62.9% of the total crustal heat flow. In other words, the radioactive heat generated by the widely distributed granitoids in western Sichuan is an important heat source for the abundant high-temperature geothermal resources.
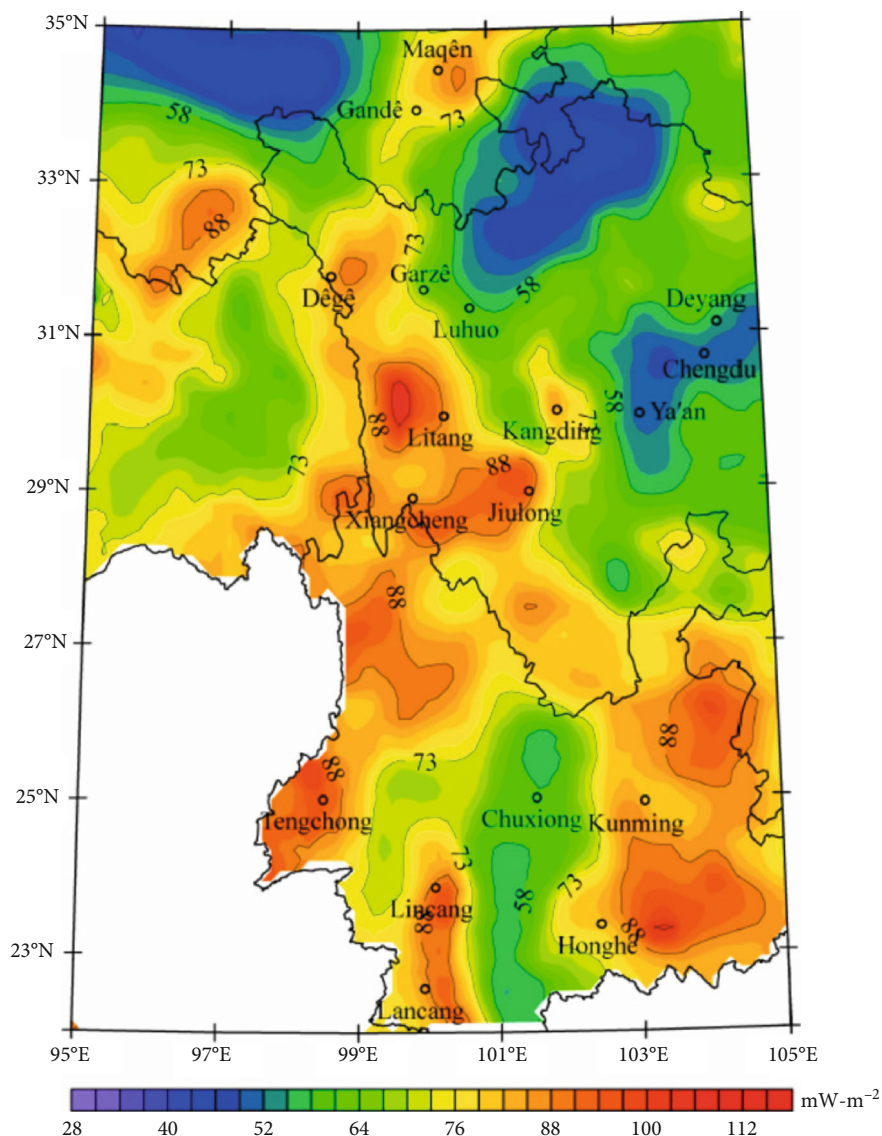
FIGURE 11: Distribution of the estimated heat flow in the southeastern Tibetan Plateau (revised from Tang et al. [68]).

The relatively large heat flow contributed by the widely distributed granitoids is due to two aspects, i.e., the relatively high RHPRs and the thickened radioactively enriched layer. The former was discussed in Section 4.1. The thickened radioactively enriched layer, which is ~10 km in the stable Craton region [38], may be related to the crustal thickening (~61 km) in the study area caused by the collision between the Indian and European plates. Such a high crustal heat flow generated by the thickened crust is also a necessary factor for the formation of the HDR geothermal resources in the Gonghe Basin, northeastern Tibetan Plateau [12].

Based on the aforementioned analysis, the important role of the granitoids in the formation of the high-temperature geothermal resources in western Sichuan is fully emphasized. Based on previous studies on the heat source and genesis mechanism, the results of this study actually reveal that the high-temperature geothermal resources in western Sichuan are characterized by multiple heat

sources, and the geothermal anomaly is related to the combined thermal contributions of all of the heat sources. This finding is consistent with the knowledge obtained in a study of HDR resources [51]. Hence, to obtain an in-depth understanding of the origin of geothermal resources (especially high-temperature geothermal resources), it is necessary to determine all of the heat sources and to reveal the corresponding heat contribution of each heat resource, which is by no means an easy task yet.

5. Conclusions

The major conclusions of this study are summarized as follows.

(1) Through the systematic compilation of the geochemical concentrations of the main granitic intrusions in western Sichuan, a total of 548 RHPR values were

obtained, which represent the first batch of RHPR data for the study area. The statistical data demonstrate that the average concentrations of the heat-producing elements U, Th, and K in the granitic rocks are 6.09 ± 5.22 ppm, 26.74 ± 16.78 ppm, and $3.51 \pm 0.82\%$, respectively. In addition, the average Th/U ratio of all of the granitic plutons is 6.02 ± 4.63

(2) The widely distributed granitic plutons in western Sichuan are characterized by a relatively broad range of heat production values, 0.52–$10.86 \, \mu W/m^3$. The arithmetic mean for all of the plutons was calculated to be $3.74 \pm 2.15 \, \mu W/m^3$, which is higher than that of global Mesozoic–Cenozoic granites. The average heat contributions of the U, Th, and K to the total heat production are 39.3%, 49.7%, and 11%, respectively

(3) The heat reservoirs of the granitic batholiths are jointly controlled by the RHPR and outcrop area. In general, the capacity to store heat increases as the RHPR and outcrop surface increase. The Dong-cuo pluton, which has an average RHPR of $2.73 \, \mu W/m^3$, possess the largest heat reservoir of 382.88×10^{13} J/a in the study area

(4) Based on the stratigraphic structure interpreted from the deep seismic sounding profile in western Sichuan, the crustal heat flow was estimated to be 48.3–$56.2 \, mW/m^2$, among which the heat flow contribution is dominated by the upper crust. The large contribution (nearly half) of the crustal heat flow to the regional background heat flow indicates that the radiogenic heat from the granitoids is an important heat source for the thermal anomaly and thus for the high-temperature geothermal resources in the study area

This study focused on the widely distributed granitoids in western Sichuan, which is one of the areas rich in high-temperature geothermal resources in China, and the thermal contribution of the granitoids to the formation of the high-temperature geothermal resources was investigated. The results of this study highlight that the granitoids serve as an important heat source. The results of this study provide an important supplement to the existing research on the heat source and genesis of the high-temperature geothermal resources conducted using various geochemical and geophysical methods. Combined with the previous results, this study indicates that western Sichuan is characterized by multiple heat sources. However, fundamental geothermal investigations in this area remain scarce, including the high-quality heat flow determinations and thermal structure studies. The lack of these key data makes it difficult to quantitatively assess the heat contribution of each heat source, hindering the obtainment of an in-depth understanding of the origin of the high-temperature geothermal resources. In future studies, more efforts should be made to increase basic knowledge and investigations, such as borehole-temperature logs, thermophysical parameter tests, heat flow determination, and deep thermal regime analysis.

Data Availability

All data analyzed in this study are available from the corresponding authors upon reasonable request.

Conflicts of Interest

The authors declare that they have no conflicts of interest.

Authors' Contributions

Chao Zhang was assigned in the conceptualization and and in writing the original draft preparation. Qingda Feng was responsible in the resources and and in writing, reviewing, and editing the manuscript. Linyou Zhang helped in writing, reviewing, and editing. Song Qing worked on the resources. Guangzheng Jiang contributed in the methodology and formal analysis. Jie Hu helped in the formal analysis. Shengbiao Hu was assigned in the methodology and supervision. Ronghua Huang worked on the investigation and helped in writing the original draft preparation. Haozhu Zhang helped in writing the original draft preparation.

Acknowledgments

References

[1] M. Rezaie and H. Aghajani, "A new combinational terminology for geothermal systems," *International Journal of Geosciences*, vol. 4, no. 1, pp. 43–48, 2013.

[2] Y. Wang, C. H. Guo, S. R. Zhuang et al., "Major contribution to carbon neutrality by China's geosciences and geological technologies," *China Geology*, vol. 4, no. 2, pp. 329–352, 2021.

[3] G. L. Wang, W. Zhang, J. Y. Liang, W. J. Lin, Z. M. Liu, and W. L. Wang, "Evaluation of geothermal resources potential in China," *Acta Geoscientica Sinica*, vol. 4, pp. 448–459, 2017.

[4] J. Tian, Z. H. Pang, Q. Guo et al., "Geochemistry of geothermal fluids with implications on the sources of water and heat recharge to the Rekeng high-temperature geothermal system in the eastern Himalayan syntax," *Geothermics*, vol. 74, pp. 92–105, 2018.

[5] J. Tian, Z. H. Pang, Y. C. Wang, and Q. Guo, "Fluid geochemistry of the Cuopu high temperature geothermal system in the eastern Himalayan syntax with implication on its genesis," *Applied Geochemistry*, vol. 110, article 104422, 2019.

[6] Y. Fan, Z. Pang, D. Liao et al., "Hydrogeochemical characteristics and genesis of geothermal water from the Ganzi geothermal field, eastern Tibetan Plateau," *Water*, vol. 11, no. 8, p. 1361, 2019.

[7] Y. Z. Cheng, Z. H. Pang, Q. Y. Di, X. B. Chen, and Y. L. Kong, "Three-dimensional resistivity structure in the hydrothermal

system beneath Ganzi Basin, eastern margin of Tibetan Plateau," *Geothermics*, vol. 93, article 102062, 2021.

[8] J. X. Li, G. Yang, G. Sagoe, and Y. L. Li, "Major hydrogeochemical processes controlling the composition of geothermal waters in the Kangding geothermal field, western Sichuan Province," *Geothermics*, vol. 75, pp. 154–163, 2018.

[9] Y. Z. Cheng, Z. H. Pang, Y. L. Kong, X. B. Chen, and G. J. Wang, "Imaging the heat source of the Kangding high-temperature geothermal system on the Xianshuihe fault by magnetotelluric survey," *Geothermics*, vol. 102, article 102386, 2022.

[10] J. Zhang, W. Y. Li, X. C. Tang et al., "Geothermal data analysis at the high-temperature hydrothermal area in western Sichuan," *Science China Earth Sciences*, vol. 60, no. 8, pp. 1507–1521, 2017.

[11] Y. F. Ai, J. Zhang, M. Dong, B. Y. Wang, and G. Fang, "Heat generation effects from shear friction along Xianshui river strike-slip fault in western Sichuan, China," *Geothermics*, vol. 89, article 101936, 2021.

[12] C. Zhang, S. B. Hu, S. S. Zhang et al., "Radiogenic heat production variations in the Gonghe Basin, northeastern Tibetan Plateau: implications for the origin of high-temperature geothermal resources," *Renewable Energy*, vol. 148, pp. 284–297, 2020.

[13] D. Chen and D. Wyborn, "Habanero field tests in the Cooper Basin, Australia: a proof-of-concept for EGS," *Geothermal Resources Council Transactions*, vol. 33, pp. 140–145, 2009.

[14] P. Baillieux, E. Schill, J. B. Edel, and G. Mauri, "Localization of temperature anomalies in the Upper Rhine Graben: insights from geophysics and neotectonic activity," *International Geology Review*, vol. 55, no. 14, pp. 1744–1762, 2013.

[15] C. Zhang, S. Hu, R. Song et al., "Genesis of the hot dry rock geothermal resources in the Gonghe Basin: constraints from the radiogenic heat production rate of rocks," *Chinese Journal of Geophysics*, vol. 63, no. 7, pp. 2697–2709, 2020.

[16] P. Z. Zhang, Q. D. Deng, G. M. Zhang et al., "Strong earthquakes activity and active blocks in mainland China," *Science in China Series D*, vol. 33, no. z1, pp. 12–20, 2003.

[17] W. Y. Li, J. Zhang, X. C. Tang, J. Tian, Y. C. Wang, and Q. Guo, "The deep geothermal structure of high-temperature hydrothermal activity region in western Sichuan Plateau: a geophysical study," *Chinese Journal of Geophysics*, vol. 61, no. 7, pp. 2926–2936, 2018.

[18] L. J. Gao, J. Zhang, and M. Dong, "The study of gravity-magnetic anomaly and tectonic background in Sichuan west region," *Chinese Journal of Geophysics*, vol. 58, no. 8, pp. 2996–3008, 2015.

[19] X. W. Xu, X. Z. Wen, R. Z. Deng, W. T. Ma, F. M. Song, and G. H. Yu, "The latest tectonic change pattern of active blocks in the Sichuan-Yunnan region and its dynamic source," *Science in China Series D*, vol. 33, no. z1, pp. 151–162, 2003.

[20] Z. W. Xu, H. Zhang, Y. Z. Hu, W. Yuan, and Y. X. Luo, "General situation and development regional division of geothermal resources in western Sichuan region," *Mineral Exploration*, vol. 10, no. 5, pp. 1233–1242, 2019.

[21] X. W. Xu, X. Z. Wen, G. H. Yu, R. Z. Zheng, H. Y. Luo, and B. Zheng, "Average slip rate, earthquake rupturing segmentation and recurrence behavior on the Litang fault zone, western Sichuan Province, China," *Science in China Series D*, vol. 48, no. 8, pp. 1183–1196, 2005.

[22] X. X. Xu, L. Y. Ji, F. Y. Jiang, and W. T. Zhang, "Study on current activity features of Jinshajiang fault zone based on GPS and small earthquakes," *Journal of Geodesy and Geodynamics*, vol. 40, no. 10, pp. 1062–1066, 2020.

[23] J. Y. Zhao, G. L. Wang, C. Y. Zhang, L. X. Xing, M. Li, and W. Zhang, "Genesis of geothermal fluid in typical geothermal fields in western Sichuan, China," *Acta Geologica Sinica*, vol. 95, no. 3, pp. 873–882, 2021.

[24] X. C. Tang, J. Zhang, Z. H. Pang, S. B. Hu, J. Tian, and S. J. Bao, "The eastern Tibetan Plateau geothermal belt, western China: geology, geophysics, genesis, and hydrothermal system," *Tectonophysics*, vol. 717, pp. 433–448, 2017.

[25] M. Luo, R. Ren, and W. Yuan, "Type, distribution and genesis of geothermal resource in Sichuan," *Acta Geologica Sichuan*, vol. 36, no. 1, pp. 47–50, 2016.

[26] Y. H. Zhang, *Research on Genesis and Development of the Geothermal System in the Kangding-Moxi Segment of the Xianshuihe Fault*, Chengdu University of Technology, Chengdu, 2018.

[27] W. Zhang, G. L. Wang, J. Y. Zhao, and L. Feng, "Geochemical characteristics of medium-high temperature geothermal fluids in west Sichuan and their geological implications," *Geoscience*, vol. 35, no. 1, pp. 188–198, 2021.

[28] C. Yuan, M. F. Zhou, M. Sun et al., "Triassic granitoids in the eastern Songpan Ganzi fold belt, SW China: magmatic response to geodynamics of the deep lithosphere," *Earth and Planetary Science Letters*, vol. 290, no. 3-4, pp. 481–492, 2010.

[29] S. Liu, Z. Wang, Q. Yan, Q. Li, D. Zhang, and J. Wang, "Timing, petrogenesis and geodynamic significance of Zheduoshan Granitoids," *Acta Petrologica Sinica*, vol. 22, no. 2, pp. 343–352, 2006.

[30] T. Wu, L. Xiao, S. A. Wilde, C. Q. Ma, and J. X. Zhou, "A mixed source for the late Triassic Garze-Daocheng granitic belt and its implications for the tectonic evolution of the Yidun arc belt, eastern Tibetan Plateau," *Lithos*, vol. 288-289, pp. 214–230, 2017.

[31] T. Wu, L. Xiao, R. Gao, H. Yang, and G. Yang, "Petrogenesis and tectonic setting of the Queershan composite granitic pluton, eastern Tibetan Plateau: constraints from geochronology, geochemistry and Hf isotope data," *Science China Earth Sciences*, vol. 57, no. 11, pp. 2712–2725, 2014.

[32] M. H. Yin, *Geochemistry and Uranium Metallogenic Condition of Granite Rocks of the Haizishan-Geinie Area in Western Sichuan*, Chengdu University of Technology, Chengdu, 2018.

[33] L. Rybach, "Radioactive heat production in rocks and its relation to other petrophysical parameters," *Pure and Applied Geophysics*, vol. 114, no. 2, pp. 309–317, 1976.

[34] I. M. Artemieva, H. Thybo, K. Jakobsen, N. K. Sørensen, and L. S. Nielsen, "Heat production in granitic rocks: global analysis based on a new data compilation GRANITE2017," *Earth-Science Reviews*, vol. 172, pp. 1–26, 2017.

[35] M. Pleitavino, M. E. Carro Pérez, E. García Aráoz, and M. A. Cioccale, "Radiogenic heat production in granitoids from the sierras de Córdoba, Argentina," *Geothermal Energy*, vol. 9, article 16, 2021.

[36] T. Veikkolainen and I. T. Kukkonen, "Highly varying radiogenic heat production in Finland, Fennoscandian shield," *Tectonophysics*, vol. 750, pp. 93–116, 2019.

[37] Z. M. Zhou, C. Q. Ma, S. H. Qi, Y. F. Xi, and W. Liu, "Late Mesozoic high-heat-producing (HHP) and high-temperature geothermal reservoir granitoids: the most significant

geothermal mechanism in South China," *Lithos*, vol. 366-367, article 105568, 2020.

[38] J. Y. Wang, *Geothermal and Its Applications*, Science Press, Beijing, 2015.

[39] K. P. Furlong and D. S. Chapman, "Heat flow, heat generation, and the thermal state of the lithosphere," *Annual Review of Earth and Planetary Sciences*, vol. 41, no. 1, pp. 385–410, 2013.

[40] X. J. Shen, S. Z. Yang, J. Y. Shen, and W. R. Zhang, "Experimental study of radiogenic heat production of granitic rocks in Tibet," *Acta Petrologica Sinica*, vol. 4, pp. 83–92, 1989.

[41] H. D. Wall, A. Schaarschmidt, M. Kämmlein, G. Gabriel, and M. Sestmann, "Subsurface granites in the Franconian Basin as the source of enhanced geothermal gradients: a key study from gravity and thermal modeling of the Bayreuth granite," *International Journal of Earth Sciences*, vol. 108, no. 6, pp. 1913–1936, 2019.

[42] R. Lamas, M. Miranda, L. Neves, and A. Pereira, "Radiogenic heat production from a deep borehole in the Beiras granite (Almeide, Central Portugal), Energy for Sustainability," *Sustainable Cities: Designing for People and the Planet*, vol. 2015, 2015.

[43] P. C. Webb, M. K. Lee, and G. C. Brown, "Heat flow - heat production relationships in the UK and the vertical distribution of heat production in granite batholiths," *Geophysical Research Letters*, vol. 14, no. 3, pp. 279–282, 1987.

[44] T. Slagstad, "Radiogenic heat production of Archaean to Permian geological provinces in Norway," *Norwegian Journal of Geology*, vol. 88, no. 3, pp. 149–166, 2008.

[45] I. T. Kukkonen and R. Lahtinen, "Variation of radiogenic heat production rate in 2.8-1.8 Ga old rocks in the central Fennoscandian shield," *Physics of the Earth and Planetary Interiors*, vol. 126, no. 3-4, pp. 279–294, 2001.

[46] L. Scharfenberg, A. Regelous, and H. D. Wall, "Radiogenic heat production of Variscan granites from the western Bohemian Massif, Germany," *Journal of Geosciences*, vol. 64, pp. 251–269, 2019.

[47] S. R. Taylor and S. M. McLennan, *The Continental Crust: Its Composition and Evolution*, , Oxford, 1985, Blackwell Scientific Publication, 1985.

[48] N. Maden and E. Akaryali, "A review for genesis of continental arc magmas: U, Th, K and radiogenic heat production data from the Gumuşhane pluton in the eastern Pontides (NE Turkiye)," *Tectonophysics*, vol. 664, pp. 225–243, 2015.

[49] A. T. Mccay and P. L. Younger, "Ranking the geothermal potential of radiothermal granites in Scotland: are any others as hot as the Cairngorms?," *Scottish Journal of Geology*, vol. 53, no. 1, pp. 1–11, 2017.

[50] Z. H. Pang, J. Luo, Y. Z. Cheng et al., "Evaluation of geological conditions for the development of deep geothermal energy in China," *Earth Science Frontiers*, vol. 27, no. 1, pp. 134–151, 2020.

[51] C. Zhang, S. B. Hu, R. H. Huang et al., "Research status of heat source mechanism of the hot dry rock geothermal resources and its implications to the studies of genetic mechanism," *Progress in Geophysics*, vol. 37, no. 5, pp. 1907–1919, 2022.

[52] K. E. Rollin, *Investigation of the geothermal potential of the UK gravity modelling of the eastern highlands granites in relation to heat flow studies,*, British Geological Survey, 1984.

[53] C. Zhang, G. Z. Jiang, Y. Z. Shi et al., "Terrestrial heat flow and crustal thermal structure of the Gonghe-guide area, northeastern Qinghai-Tibetan Plateau," *Geothermics*, vol. 72, pp. 182–192, 2018.

[54] Q. Yan, A. J. Wang, G. S. Wang, W. J. Yu, and Q. S. Chen, "Resource evaluation of global geothermal energy and the development obstacles," in *2010 International Conference on Advances in Energy Engineering*, Beijing, 2010.

[55] F. Lucazeau, "Analysis and mapping of an updated terrestrial heat flow data set," *Geochemistry, Geophysics, Geosystems*, vol. 20, no. 8, pp. 4001–4024, 2019.

[56] C. Y. Wang, W. B. Han, J. P. Wu, H. Lou, and W. W. Chan, "Crustal structure beneath the eastern margin of the Tibetan Plateau and its tectonic implications," *Journal of Geophysical Research*, vol. 112, no. B7, article B07307, 2007.

[57] A. H. Lachenbruch, "Crustal temperature and heat production: implications of the linear heat-flow relation," *Journal of Geophysical Research*, vol. 75, no. 17, pp. 3291–3300, 1970.

[58] L. Rybach and G. Buntebarth, "The variation of heat generation, density and seismic velocity with rock type in the continental lithosphere," *Tectonophysics*, vol. 103, no. 1-4, pp. 335–344, 1984.

[59] V. Čermák and L. Bodri, "A heat production model of the crust and upper mantle," *Tectonophysics*, vol. 194, no. 4, pp. 307–323, 1991.

[60] J. Sun, G. W. Jin, D. H. Bai, and L. F. Wang, "Exploration of the electrical structure in the crust and upper mantle in eastern margin of Tibetan Plateau and its geotectonic implications," *Science in China Series D*, vol. 33, no. z1, pp. 173–180, 2003.

[61] J. W. Teng, D. H. Yang, X. B. Tian et al., "Geophysical investigation progresses of the Qinghai-Tibetan Plateau in the past 70 years," *Scientia Sinica Terrae*, vol. 49, no. 10, pp. 1546–1564, 2019.

[62] G. Z. Jiang, P. Gao, S. Rao et al., "Compilation of heat flow data in the continental area of China (4th edition)," *Chinese Journal of Geophysics*, vol. 59, no. 8, pp. 2892–2910, 2016.

[63] S. B. Hu, L. J. He, and J. Y. Wang, "Compilation of heat flow data in the China continental area (3rd edition)," *Chinese Journal of Geophysics*, vol. 44, no. 5, pp. 604–618, 2001.

[64] L. M. Wen, G. F. Kang, C. H. Bai, and G. M. Gao, "Studies on the relationships of the curie surface with heat flow and crustal structures in Yunnan Province, China, and its adjacent areas," *Earth, Planets and Space*, vol. 71, no. 85, pp. 1–19, 2019.

[65] Y. Okubo, H. Tsu, and K. Ogawa, "Estimation of curie point temperature and geothermal structure of island arcs of Japan," *Tectonophysics*, vol. 159, no. 3-4, pp. 279–290, 1989.

[66] J. L. C.-D. L. Cruz, R. M. Prol-Ledesma, D. Gómez-Rodríguez, and A. A. Rodríguez-Díaz, "Analysis of the relation between bottom hole temperature data and curie temperature depth to calculate geothermal gradient and heat flow in Coahuila, Mexico," *Tectonophysics*, vol. 780, article 228397, 2020.

[67] Y. Okuboi and T. Matsunaga, "Curie point depth in northeast Japan and its correlation with regional thermal structure and seismicity," *Journal of Geophysical Research*, vol. 99, no. B11, pp. 22363–22371, 1994.

[68] H. H. Tang, L. H. Guo, and Y. Fang, "Estimation of heat flow in southeastern margin of Tibetan Plateau and its analysis of the correlation with earthquake activity," *Chinese Journal of Geophysics*, vol. 63, no. 3, pp. 1056–1069, 2020.